Noorhana Yahya

ADVANCED STRUCTURED MATERIALS 5

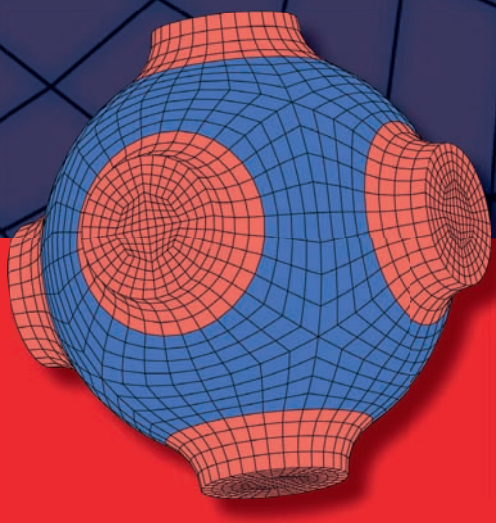

Carbon and Oxide Nanostructures

Synthesis, Characterisation and Applications

Springer

Advanced Structured Materials

Volume 5

For further volumes:
http://www.springer.com/series/8611

Noorhana Yahya

Carbon and Oxide Nanostructures

Synthesis, Characterisation and Applications

Springer

Assoc. Prof. Dr. Noorhana Yahya
Department of Fundamental and Applied Sciences
Universiti Teknologi PETRONAS
Bandar Seri Iskandar
31750 Tronoh, Perak
Malaysia
noorhana_yahya@petronas.com.my

ISSN 1869-8433
ISBN 978-3-642-14672-5 e-ISBN 978-3-642-14673-2
DOI 10.1007/978-3-642-14673-2
Springer Heidelberg Dordrecht London New York

Library of Congress Control Number: 2010937766

Cover design: WMXDesign GmbH, Heidelberg, Germany

Printed on acid-free paper

Springer is part of Springer Science+Business Media (www.springer.com)

Preface

It is my privilege as the Editor-in-Chief to present to you an effort of our team of prominent contributors to this monograph on Carbon and Oxide Nanostructures. Over the past 20 years, carbon and oxide nanostructures evolved into one of the most studied objects and are presently entering in the transition phase from nanoscience to nanotechnology. Carbon and oxide nanostructures constitute an enormous topic which may only be described in a simplified manner, which in essence is the intent of this book. It is hoped that this book would provide valuable resources for researchers as well as postgraduate students of physics, chemistry and engineering. Related carbon-based materials such as fullerenes, carbon fiber, glassy carbon, carbon black, amorphous carbon, diamond, graphite, buckminsterfullerene, and carbon nanotubes (CNTs) are discussed. CNTs which have attracted the attention of the scientific community due to their fundamental and technical importance are elaborated. It also presents a review of the applications of fullerene and its derivatives as electron beam resists, as well as outlining the effects of catalyst on the morphology of the carbon nanotubes. Structural and optical properties of hydrogenated amorphous carbon (a-C:H) thin films prepared in a DC-plasma-enhanced chemical vapor deposition reactor is discussed in greater detail. Some of the works done on polymer-CNTs-based solar cells with a variety of device architecture and band diagram are summarized. Several irregular configurations of carbon nanofibers (CNF) such as coiled, regular helical, and twisted coil are elaborated. This book also includes the molecular modeling of carbon-based nanomaterials including discussions on some aspects of the issues related to the synthesis and characterization of diamond prepared via CVD techniques using the hot filaments and plasma. Oxide-based materials related to fuel synthesis and solar hydrogen production are also presented. The versatility of ZnO nanostructures and some of the novel applications such as solar cells and light-emitting devices are being highlighted. A brief introduction of Fe–FeO nanocomposites and some superparamagnetism studies in the form of particles and thin films are included. The benefits and drawbacks of the properties of some nanomaterials used in optical sensing applications are given, and the recently developed optical chemical sensors and probes based on photoluminescence are also rigorously overviewed. Aspects of nanocatalytic reactions, the types of catalyst, and also the preparation and characterization of the active catalyst for ammonia synthesis are scrutinized.

I am grateful to all authors who have contributed to the chapters of this book. All merits on overview of such an enormous topic as Carbon and Oxide Nanostructures in this concise monograph should be credited to all contributing authors, but any shortcomings to be attributed to the Editor-in-Chief. The book is dedicated with all sincerity to all whose work has not received due reference and recognition.

Universiti Teknologi PETRONAS Assoc. Prof. Dr. Noorhana Yahya
Malaysia

Contents

Carbon Nanotubes: The Minuscule Wizards 1
Noorhana Yahya and Krzysztof Koziol

Synthesis of Carbon Nanostructures by CVD Method 23
Krzysztof Koziol, Bojan Obrad Boskovic, and Noorhana Yahya

Fullerene (C60) and its Derivatives as Resists for Electron Beam Lithography 51
Hasnah Mohd Zaid

Hydrogenated Amorphous Carbon Films 79
Suriani Abu Bakar, Azira Abdul Aziz, Putut Marwoto, Samsudi Sakrani, Roslan Md Nor, and Mohamad Rusop

Carbon Nanotubes Towards Polymer Solar Cell 101
Ishwor Khatri and Tetsuo Soga

Irregular Configurations of Carbon Nanofibers 125
Suriati Sufian

Molecular Simulation to Rationalize Structure-Property Correlation of Carbon Nanotube 143
Abhijit Chatterjee

Carbon Nanostructured Materials 165
Azira Abdul Aziz, Suriani Abu Bakar, and Mohamad Rusop

Diamond: Synthesis, Characterisation and Applications 195
Roslan Md Nor, Suriani Abu Bakar, Tamil Many Thandavan, and Mohamad Rusop

Versatility of ZnO Nanostructures 219
Muhammad Kashif, Majid Niaz Akhtar, Nadeem Nasir, and Noorhana Yahya

Supported Nanoparticles for Fuel Synthesis 245
Noor Asmawati Mohd Zabidi

Nanotechnology in Solar Hydrogen Production 263
Balbir Singh Mahinder Singh

Fe–FeO Nanocomposites: Preparation, Characterization and Magnetic Properties 281
Jamshid Amighian, Morteza Mozaffari, and Mehdi Gheisari

Nanostructured Materials Use in Sensors: Their Benefits and Drawbacks 307
Aleksandra Lobnik, Matejka Turel, Špela Korent Urek, and Aljoša Košak

Zinc Oxide Nanostructured Thin Films: Preparation and Characterization 355
Mohamad Hafiz Mamat and Mohamad Rusop

Superparamagnetic Nanoparticles 375
Boon Hoong Ong and Nisha Kumari Devaraj

Ammonia Synthesis 395
Noorhana Yahya, Poppy Puspitasari, Krzysztof Koziol, and Pavia Giuseppe

Carbon Nanostructured Materials

Azira Abdul Aziz, Suriani Abu Bakar, and Mohamad Rusop

Abstract In recent years, a lot of work has been focused on the synthesis of novel materials, clusters, and molecules which are unique in many ways. Numerous attempts to synthesize the theoretically predicted solids have been published. This chapter summarised the carbon materials in various forms; crystalline and non-crystalline. Carbon constitutes a class of new materials with a wide range of compositions, properties, and performance. Due to its unique optical and electrical properties, carbon has potential applications in vast fields especially in semiconductor devices. The structure and properties of the various crystalline carbon materials are reviewed. Related carbon based materials such as fullerenes, carbon fiber, glassy carbon, carbon black, amorphous carbon, diamond, graphite and buckminsterfullerene mentioned briefly as well as carbon nanotubes (CNTs). The CNTs preparation and characterization methods are presented and discussed in depth. However, it can be stated that a fascinating new field in the area of carbon has been discovered, which gives motivation for further studies dedicated to fundamental questions as well as the exploitation of the novel materials for industrial applications.

A.A. Azira (✉) and S.A. Bakar
NANO-SciTech Centre, Institute of Science, Universiti Teknologi MARA, 40450 Shah Alam, Selangor, Malaysia
Faculty of Applied Sciences, Universiti Teknologi MARA, 40450 Shah Alam, Selangor, Malaysia
e-mail: aziraaziz@yahoo.com; absuriani@yahoo.com
M. Rusop
NANO-SciTech Centre, Institute of Science, Universiti Teknologi MARA, 40450 Shah Alam, Selangor, Malaysia
Faculty of Electrical Engineering, Solar Cell Laboratory, Universiti Teknologi MARA, 40450 Shah Alam, Selangor, Malaysia
e-mail: rusop8@gmail.com

N. Yahya (ed.), *Carbon and Oxide Nanostructures,* Adv Struct Mater 5,
DOI 10.1007/8611_2010_14,
Published online: 26 June 2010

1 Introduction

Carbon has been known since ancient times in the form of soot, charcoal, graphite and diamonds. Ancient cultures did not of course realize that these substances were different forms of the same element. 'Carbon' is derived from the Latin carbo, meaning charcoal. Carbon based materials, clusters and molecules are unique in many ways and allotropes of carbon are inter convertible to each other suitable temperature and pressure. Carbon is most commonly obtained from coal deposits, although it usually must be processed into a form suitable for commercial use. Three naturally occurring allotropes of carbon are known to exist: amorphous, graphite and diamond. Under ambient condition, the graphite phase with strong in-plane trigonal bonding is a stable phase. Under high pressure (60,000 atm) and temperature (2,000 K) graphite can be converted to diamond and when exposed to irradiation or heat, diamond will quickly transform back to the more stable graphite phase. Carbon has atomic number of 6 and is classified in group IV of the second period of the periodic table and has $1s^2 2s^2 2p_x^1 p_y^1$ electronic ground state configuration. In the graphite structure, strong in plane bonds are formed which is denoted by trihedral sp^2 and in diamond structure, they are tetrahedrally bonded sp^3 configuration.

2 Carbon Structures

Carbon is a fascinating and very unique element because it can assume various forms and structures. It is very abundant and is the basis of organic life. Carbon has two features which, taken together, make it quite unique: a carbon atom can bond with another carbon atom in several configurations (different hybridizations of the C-C bond), and can also bond with many other elements, among those hydrogen, nitrogen and oxygen. In order to understand the nature of the carbon bond it is necessary to examine the electronic structure of the carbon atom. Carbon contains six electrons, which are distributed over the lowest energy levels of the carbon atom. The structure is designated as follows ($1s^2$), (2s), ($2p_x$), ($2p_y$), ($2p_z$) when bonded to atoms in molecules electron. The configuration of ground state (lowest energy state) of carbon is shown in Fig. 1 below.

The lowest energy level 1s with the quantum number $N = 1$ contains two electrons with oppositely paired electron spins. The electron charge distribution in an s state is spherically symmetric about the nucleus. The 1s electrons do not participate in the chemical bonding. The next four electrons are in the $N = 2$ energy state, one in a spherically symmetric s orbital, and three in p_x, p_y, and p_z orbitals,

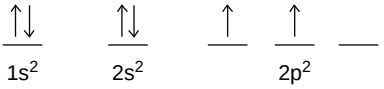

Fig. 1 The configuration of ground state (lowest energy state) of carbon

which have the very directed charge distributions shown in Fig. 1, oriented perpendicular to each other. The outer s orbital together with the three p orbitals form the chemical bonds of carbon with other atoms. The charge distribution associated with these orbitals mixes (or overlaps) with the charge distribution of each other atom being bonded to the carbon. In effect, the electron charge between the two carbon atoms of a bond can be viewed as the glue that holds the atoms together.

From the ground state electron configuration, one can see that carbon has four valence electrons, two in the 2s subshell and two in the 2p subshell. The 1s electrons are considered to be core electrons and are not available for bonding. There are two unpaired electrons in the 2p subshell, so if carbon were to hybridize from this ground state, it would be able to form at most two bonds. Recall that energy is released when bonds form, so it would be to carbon's benefit to try to maximize the number of bonds it can form. For this reason, carbon will form an excited state by promoting one of its 2s electrons into its empty 2p orbital and hybridize from the excited state. By forming this excited state, carbon will be able to form four bonds. The excited state configuration is shown in Fig. 2 below.

In order to determine the hybridization on a carbon atom, Lewis structure must be drawn. From the Lewis structure, the numbers of groups around the central carbon need to be counted. A group represents the regions of electron density around the carbon, and may be single, double or triple bonded. The number of groups represents how many hybrid orbitals have formed. The number of hybrid orbitals formed equals the number of atomic orbitals mixed. The description of the atomic orbitals mixed is equivalent to the hybridization of the carbon atom.

The Lewis structure shows four groups around the carbon atom. This means four hybrid orbitals have formed. In order to form four hybrid orbitals, four atomic orbitals have been mixed. The s orbital and all three p orbitals have been mixed, thus the hybridization is sp^3. By using the atomic orbitals of excited state carbon found in the valence shell. The four sp^3 hybrid orbitals will arrange themselves in three dimensional space to get as far apart as possible (to minimize repulsion). The geometry that achieves this is tetrahedral geometry, where any bond angle is 109.5° as described in Fig. 3.

Each hybrid orbital contains one electron. A hydrogen 1s orbital will come in and overlap with the hybrid orbital to form a sigma bond (head-on overlap). The Lewis structure shows three groups around each carbon atom. This means three hybrid orbitals have formed for each carbon. In order to form three hybrid orbitals, three atomic orbitals have been mixed. The s orbital and two of the p orbitals for each carbon have been mixed, thus the hybridization for each carbon is sp^2. By referring to Fig. 4, using the atomic orbitals of excited state carbon found in the valence shell.

The three sp^2 hybrid orbitals will arrange themselves in three dimensional space to get as far apart as possible. The geometry that achieves this is trigonal planar

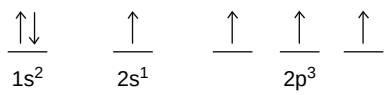

Fig. 2 The excited state configuration of carbon

Fig. 3 The sp^3 hybridization structure (three-dimension)

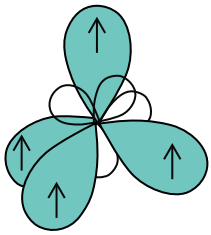

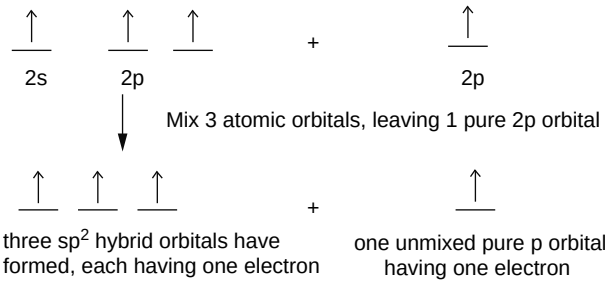

Fig. 4 The schematic diagram of sp^2 hybrid orbitals

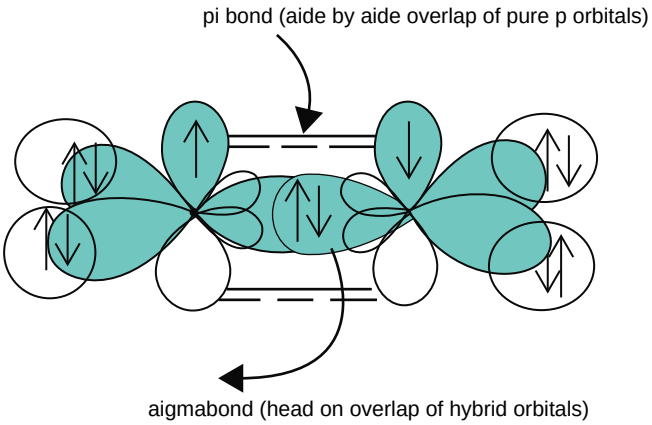

Fig. 5 The head-on overlap of sp^2 orbitals

geometry, where the bond angle between the hybrid orbitals is 120°. The unmixed pure p orbital will be perpendicular to this plane and each carbon atom is sp^2, and trigonal planar as shown in Fig. 5.

The head-on overlap of sp^2 orbitals forms a bond and the side by side overlap of pure p orbitals forms a pi bond between the carbon atoms. This accounts for the carbon-carbon double bond. Each carbon is trigonal planar with a bond angle of 120°. By referring to acetylene, C_2H_2 the Lewis structure, shows two groups around

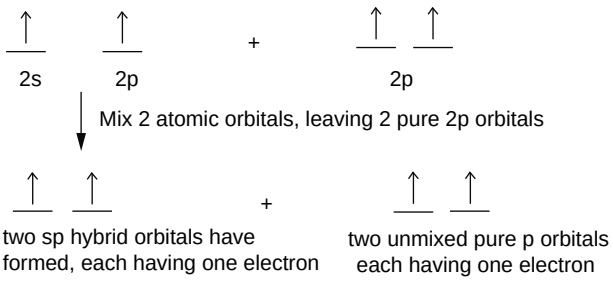

Fig. 6 The schematic diagram of two sp hybrid orbitals

each carbon atom. This means two hybrid orbitals have formed. In order to form two hybrid orbitals, two atomic orbitals have been mixed. By using the atomic orbitals of excited state carbon found in the valence shell as shown in Fig. 6.

The two sp hybrid orbitals arrange themselves in three dimensional space to get as far apart as possible. The geometry which achieves is linear geometry with a bond angle of 180°. The two pure p orbitals which were not mixed are perpendicular to each other. The triple bond consists of one sigma bond and two pi bonds. The geometry around each carbon is linear with a bond angle of 180°.

Solid carbon has two main structures called allotropic forms that are stable at room temperature: diamond and graphite. Diamond consists of carbon atoms that are tetrahedrally bonded to each other through sp^3 hybrid bonds that form a three dimensional network. Each carbon has four nearest-neighbour carbons. Graphite has a layered structure with each layer, called a graphite sheet, formed from hexagons of carbon atoms bound together by sp^2 hybrid bonds that make 120° angles with each other. Each carbon atom has three nearest-neighbour carbons in the planar layer. The hexagonal sheets are held together by weaker van der Waals forces. Van der Waals forces exists from the clusters of gases tend to be larger because of their atoms have closed shells that are held together by much weaker forces.

Crystalline carbon can be found in essentially two forms in nature, namely graphite and diamond. They correspond to two different ways of forming a bond between carbon atoms, namely the sp^2 (typical of graphite, with three nearest neighbours arranged in the same plane) and sp^3 bond (typical of diamond, with four nearest neighbours located at the tips of a regular tetrahedron). Although they are both formed of pure carbon, their chemical and physical properties are very different and in some aspects completely opposite. In graphite, the planar graphene sheets of sp^2-bonded carbon atoms glide easily in a direction parallel to the planes, resulting in a very soft material while diamond is among the hardest materials known. Graphite is a zero gap semiconductor while diamond is a high band gap semiconductor. Graphite is opaque, while diamond is transparent. It exists in different allotropic forms that give rise to its versatile behavior. In the amorphous form it is powdery in nature and black in color. It becomes the hardest substance known and has a shining appearance in the allotropic form of diamond. Catenation, the self-linking property of carbon atoms is responsible for much of organic

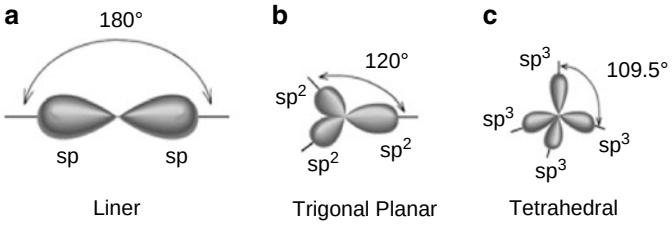

Fig. 7 The different hybridisations of carbon (**a**) sp^1, (**b**) sp^2, (**c**) sp^3

chemistry. The role of carbon clusters and carbon clouds in the interstellar region and in atmosphere remains to be understood [1]. In 1980, only three forms of carbon, namely diamond, graphite and amorphous (non-crystalline carbon).

The chemical element carbon can combine with itself and other elements in three types of hybridisations. This gives the rich diversity of structural forms of solid carbon and is the basis of organic chemistry and life. In the sp^3 hybridisation four equivalent $2sp^3$ hybrid orbitals are tetrahedrally oriented around the atom (Fig. 7) and can form four equivalent σ bonds by an overlap with orbitals of other atoms. An example is the ethane molecule (C_2H_6) where a Csp^3-Csp^3 σ bond (or C-C) is formed between two carbon atoms by the overlap of sp^3 orbitals, and three Csp^3-H1s σ bonds are formed on each C atom. In the sp^2 hybridisation three equivalent $2sp^2$ orbitals are formed and one unhybridised 2p orbital is left. They are coplanar and oriented at 120° to each other and form σ bonds by an overlap with orbitals of neighbouring atoms as e.g. in ethane (C_2H_4). The remaining p orbitals on each C atom form a π bond by the overlap with the π orbital from the neighbouring C atom. Such bonds formed between two C atoms are represented as Csp^2=Csp^2 (or C=C). Figure 7 shows the different hybridisations of carbon sp^1, sp^2 and sp^3.

In the sp^1 hybridisation two linear $2sp^1$ orbitals are formed and two 2p orbitals are left. Linear σ bonds are formed by the overlap of the $2sp^1$ hydride orbitals of neighbouring atoms as for example in the ethyne molecule (acetylene). Two π bonds are formed with the overlapping unhybridised π orbitals of the two C atoms. These bonds are represented as Csp ≡ Csp (or C ≡ C). In the aromatic carbon-carbon bond exemplified by the aromatic molecule benzene (C_6H_6) the carbon atoms are bonded with sp^2 σ bonds in a regular hexagon. The ground state π orbitals are all bonding orbitals and are fully occupied; there is a large delocalisation energy that contributes to the stability of the molecule. The aromatic carbon-carbon bond is denoted as Car ≅ Car.

3 New Carbon Structures

Until 1964 it was generally believed that no other carbon bond angles were possible in hydrocarbon, that is, compound containing only carbon and hydrogen atoms. In that year Phil Eaton of the University of Chicago synthesized a square carbon

Table 1 Types of sp^n hybridization, the resulting bond angles, and examples of molecules

Types of hybridization	Diagonal sp	Trigonal sp^2	Tetrahedral sp^3
Orbital used for bond	s, p_x	s, p_x, p_y	s, p_x, p_y, p_z
Example	Acetylene C_2H_2	Ethylene C_2H_4	Methane CH_4
Bond angle	109°28′	180°	120°

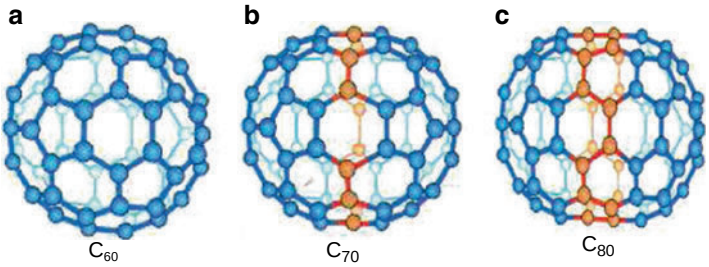

Fig. 8 Structure of (**a**) fullerene, C_{60}, (**b**) C_{70} and (**c**) C_{80} [2]

molecule, C_8H_8, called cubane. In 1983, L. Paquette of Ohio State University synthesized a $C_{20}H_{20}$ molecule having a dodecahedron shape, formed by joining carbon pentagons, and having C-C bond angles ranging from 108° to 110°. The synthesis of these hydrocarbon molecules with carbon bond angles different from standard hybridization values of Table 1 has important implication for the formation of carbon nanostructures, which would also require different bonding angles.

3.1 Fullerenes

Today there are whole families of other forms of carbon. Laser evaporation of a carbon substrate using the apparatus in a pulse of He gas can be used to make carbon clusters. The neutral cluster beam is photoionized by a UV laser and analyzed by mass spectrometer. The first of these to be discovered was buckminsterfullerene (also called buckyball and fullerene C_{60}). The discovery of fullerene [2], a new form of carbon, was perhaps a serendipity. But it led to a number of other fundamental discoveries. Fullerenes of various sizes and shapes have been reported subsequently. It would be fair to say that the discovery of carbon nanotubes in 1991 was a by-product of the fullerene production process [3].

The discovery of the existence of a soccer-ball-like molecule containing 60 carbon atoms was named fullerene. Fullerene C_{60}, (buckyball), is the first spherical carbon molecule with carbons arranged in a soccer ball shape (Fig. 8). In the structure there are 60 carbon atoms (hence C_{60}) and a number of five-membered rings isolated by six-membered rings [4]. It may well be that these objects can be used as ball bearings in some of Drexler's mechanical devices. The second

spherical carbon molecule in the same group is the rugby ball, C_{70}, whose structure has extra six-membered carbon rings (Fig. 8), but there are also a large number of other potential structures containing the same number of carbon atoms (isomers) depending on whether five-membered rings are isolated or not, or whether seven-membered rings are present. Many other forms of fullerenes up to and beyond C_{120} have been characterized and it is possible to draw lots of structure with five-membered rings in different positions and sometimes together.

The important fact for nanotechnology is that the atom can be placed inside the fullerene ball. Atoms contained within the fullerene are aid to be endohedral and they can also be bound to fullerenes outside the ball as salts if the fullerene can gain electrons. The structure is then $M_x^+C_{60}^{n-}$, where M^+ is a cation and x is the number to balance the charge on the fullerene. In this case the cation is said to be exahedral [5–8].

A sketch of the molecule is shown in Fig. 8. It has 12 pentagonal (five sided) and 20 hexagonal (six sided) faces symmetrically arrayed to form a molecular ball. The ball-like molecules bind with each other in the solid state to form a crystal lattice having a face centered cubic structure. In the lattice each C_{60} is separated from its nearest neighbour by 1 nm (the distance between their centers is 1 nm), and they are held together by van der Waals forces. Larger fullerenes such as C_{70}, $C_{76,}$ C_{80} and C_{84} have also been found. The interesting about the fullerene is, in practical terms, they many have a number of applications. For example, they have been used as lubricants because the tiny balls can roll between surfaces (it turns out that pure fullerenes are not good for this; they must be changed chemically first by having other atoms bonded around the ball). Also, they turn out to have strong optical effects (i.e. they change their properties upon irradiation with light, UV, in most cases), which could be useful in photolithography.

3.2 Carbon Fibers

Carbon fibers represent important class of graphite-related materials. Many precursors can be used to synthesize carbon fibers with high mechanical strength, each having different cross-sectional morphologies, when the as-prepared vapor-grown fibers were heat-treated to 3,000°C, forms facets, of all carbon fibers. These faceted are closest to crystalline graphite in both crystal structure and properties [9].

3.3 Glassy Carbon

Glassy carbon (GC) is another common material, which is manufactured as a commercial product by slow, controlled degradation of certain polymers at temperature typically on the order of 900–1,000°C [10]. The name glassy carbon is thus given to family of disordered carbon materials, which are glass-like and can be easily polished to attain a black, shiny appearance.

3.4 Carbon Black

Classical carbon blacks represent many types of finely divided carbon particles that are produced by hydrocarbon dehydrogenation [10, 11] and are widely used in industry as a filler to modify the mechanical, electrical, and optical properties of the materials in which they are dispersed [10, 12]. Various types of industrial carbon blacks are produced by various methods for example; thermal blacks are typically obtained by thermal decomposition of nature gas, channel blacks by partial combustion of natural gas, etc. One of the characteristic signatures associated with carbon blacks is a concentric organization of the graphite layers in each individual particle.

3.5 Amorphous Carbon

In addition to the crystal carbon, non-crystalline carbon constitutes a class of new materials with a wide range of composition, properties, and performance. This field of non-crystalline carbon is of interest both technologically to materials scientists and also at a more fundamental level to solid-state chemists and physicists. The physical properties of the various non-crystalline forms of carbon are compared with those of diamond, graphite and C_{60} in Table 2.

Non-crystalline carbon mainly include amorphous carbon (a-C) and amorphous hydrogenated carbon (a-C:H). a-C and A-C:H refer to highly disordered network of carbon atoms having no long-range order, but some short-range order, can be considered to be intermediate between diamond, graphite and hydrocarbon polymers, in that they can contain variable amounts of sp^2 and sp^3 sites and hydrogen. Since the nature of short-range order varies significantly from one preparation method to another, the properties of amorphous carbon likewise vary according to preparation method [13]. Two parameters, the carbon bonding and the hydrogen content, are most sensitive for characterizing the short-range order, which many exist on a length scale of ~10 A. Thus the sp^2-bonded carbons of a-C may cluster into tiny warped layered regions; the sp^3-bonded carbon may also cluster and segregate, as may the hydrogen impurities, which are very effective in passivating the dangling bonds.

Table 2 Properties of various forms of carbon

Materials	Density (g cm^{-3})	Hardness (GPa)	% sp^3	at. %H	Energy (Gap eV)
Diamond	3.515	100	100		5.5
Graphite	2.267		0		0.04
C_{60}			0	0	1.8
Glassy C	1.3–1.55	2–3	~0		0.01
a-C, evap	1.9–2.0	2–5	1		0.4–0.7
a-C, MSIB	3.0	30–130	90 ± 5	<9	0.5–1.5
Pda-C:H, hard	1.6–2.2	10–20	30–60	10–40	0.8–1.7
Pda-C:H, soft	0.9–1.6	<5	50–80	40–65	1.6–4
Polyethylene	0.92	0.01	100	67	6

The introduction of disorder and sp^3 defects creates a semiconductor with localized states near the Fermi level and an effective band gap between mobile filled valence band states and empty conduction states. The greater is the disorder, the greater the concentration of sp^3 bonds.

a-C and a-C:H have been prepared by variety of deposition method, such us chemical vapor deposition, ion beam sputtering, laser plasma etc. The properties of the amorphous carbon are strongly dependent on the deposition technique, e.g. amorphous carbon prepared by evaporation tends to have smaller band gap ($E_g \sim 0.4$–0.7 eV) compared with that of prepared by ion deposition for which the E_g is in the range of range of 0.4–0.3 eV [14, 15].

3.6 Diamond

Diamond exists in a cubic and hexagonal form (Lonsdaleite). In the most frequent cubic form each carbon atom is linked with four other carbon atoms by four sp^3 σ bonds in a tetrahedral array with a C-C bond length of 1.544 Å [16]. This is nearly 10% larger than in graphite. However the atomic density (1.77×10^{23} cm^{-3}) is 56% higher than in graphite. The crystal structure is zinc blend type (FCC) with a diatomic basis. The second carbon atom is at position (¼, ¼, ¼) in the unit cell and the lattice constant is $a_0 = 3.567$ Å (Fig. 9a). The physical properties of diamond are given by its structure.

Diamond is a wide-gap semiconductor (5.47 eV), the hardest material in nature (Most hardness 10) and has the highest atomic density. Diamond, as also graphite (in-plane) have the highest thermal conductivity (~25 W cm^{-1} K^{-1}) and the highest melting point (4,500 K). The hexagonal diamond (Lonsdaleite) has a wurtzite crystal structure (Fig. 9, right) and a C-C bond length of 1.52 Å [16]. The gravimetric density of both types of diamond is 3.52 g cm^{-3}.

3.7 Graphite

In graphite the atoms are arranged in layers of a honeycomb network in which the carbon atoms are bonded with sp^2 σ bonds and a delocalized π bond. In the most common hexagonal crystal form of graphite the layers are stacked in an ABAB... sequence (called Bernal stacking) (Fig. 10). The in-plane nearest neighbour distance aC-C is 1.421 Å [17] and the lattice constant is $a_0 = 2.461$ Å. The c-axis lattice constant is $c_0 = 6.708$ Å and the interplanar distance $c_0/2$. A minor component of well-crystallised graphite is the rhombohedral form of graphite in which the graphene (single layer of crystalline graphite) layers are stacked in the ABCABC... sequence. The lattice constant is also $a_0 = 2.456$ Å and $c_0 = 3\ (3.438) = 10.044$ Å. The Bernal AB stacking of graphite is more stable than the ABC stacking. The density of both forms of graphite is 2.26 g cm^{-3} [18]. The weak interlayer bonding of graphite originates from the small overlap of the π-orbitals between atoms of adjacent layers and not to Van der Waals bonding [19].

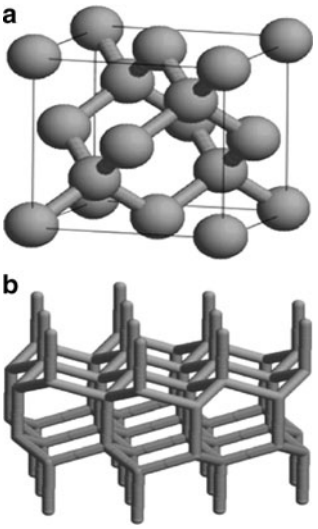

Fig. 9 Diamond in (**a**) cubic form and (**b**) hexagonal Lonsdaleite

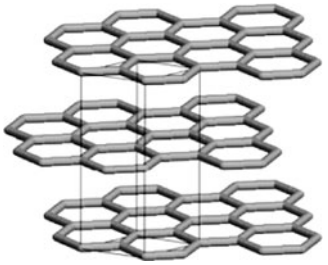

Fig. 10 Hexagonal graphite (ABAB stacking) with unit cell

3.8 Buckminsterfullerenes

Experimental and theoretical work has shown that the most stable form of carbon clusters form linear chains [20] for clusters of up to about 10 atoms. For clusters that have 10 to 30 carbon atoms the ring is the most stable form [21]. Carbon clusters between 30 and 40 carbon atoms are unlikely and clusters above 40 atoms form cage structures. Especially stable structures are the C_{60} (Fig. 11), whose structure was identified the first time by Kroto et al. in 1985 [8]. The carbon atoms are located at the 60 vertices of a truncated icosahedron that has 90 edges and 32 faces of which 12 are pentagons and 20 hexagons, consistent with Euler's theorem for polyhedra:

$$f + v = e + 2 \tag{1}$$

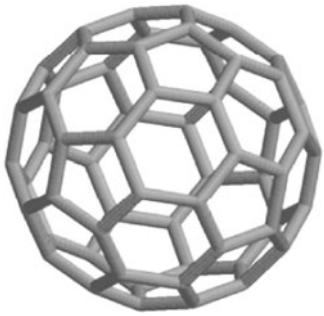

Fig. 11 C_{60} Buckminsterfullerene

where *f*, *v* and *e* are the number of faces, vertices, and edges of the polyhedra. The average nearest-neighbour C-C distance is with aC-C = 1.44 Å almost equal to that in graphite. Each carbon atom is trigonally bonded to three other carbon atoms in an sp^2-derived bonding configuration. The curvature of the trigonal bonds in C_{60} leads to some admixture of sp^3 bonding, characteristic for tetrahedrally bonded diamond, but absent in graphite [22]. Further stable fullerenes are C_{70}, C_{78} and C_{80}.

3.9 Carbon Nanotubes

Carbon nanotubes are cylindrical molecules ~1 nm in diameter and 1–100 μm in length. They are constituted of a hexagonal network of carbon atoms and can essentially be thought of as a layer of graphite rolled-up into a cylinder [3]. Properties of the nanotube researched include the different arrangements of the nanotube hexagonal structure such as the zigzag and the armchair. Carbon nanotubes are the strongest fibers known. A single perfect nanotube is about 10–100 times stronger than steel per unit weight. A carbon nanotube is synthesized through three methods: the carbon arc method where ordered nanotubes are produced from ionized carbon plasma, the laser vaporization of carbon targets and catalytic vapor deposition. A new method proposed by the authors for growing carbon nanotubes from renewable material is fluidized floating catalyst method [23–27]. Currently, carbon nanotubes can be applied as semiconductors for transistors, space transportation and data storage for computers. The carbon nanotube is still currently under heavy research and many possible applications are being conceived. Carbon nanotubes are constituted of a hexagonal network of carbon atoms and can essentially be thought of as a layer of graphite rolled-up into a cylinder (a commonly mentioned noncarbon variety is made of boron nitride) a distinction between multi-walled and single-walled nanotubes. Carbon nanotubes can also come in circular form. Carbon nanotubes surprisingly have very high tensile strength and they have varying electrical properties, which depending on the way the graphite sheet is being rolled up and other factors), and can be insulating, semiconducting or conducting (metallic).

Currently, the physical properties are still being discovered and disputed. What makes it so difficult is that nanotubes have a very broad range of electronic, thermal, and structural properties that change depending on the different kinds of nanotube (defined by its diameter, length, and chirality. Nanotubes can either act as electrical conductors, semiconductors or insulators. This makes them very good choices for nanoscale wires and electrical components. Nanotubes exhibit electrical conductivity as high as copper, thermal conductivity as high as diamond and strength 100 times greater than steel at one sixth the weight. Carbon nanotubes are quite popular now for their prospective electrical, thermal, mechanical and chemical applications.

Carbon nanotubes can be thought to be formed by the rolling of graphite layers. The rolling of a single layer of graphite results in a single-walled carbon nanotube (SWCNT), whereas the rolling of more than one layer around a central axis produces multi-walled carbon nanotubes (MWCNT). Depending on the way of rolling of graphene sheets (as shown in Fig. 12), nanotubes of different types, viz. armchair, zig-zag and chiral could be produced. They can be represented using the method given by Hamada et al. [28]. For example, to realize an (n, m) nanotube, one has to move n times a_1 from the selected origin and then m times a_2. On rolling the graphite sheet these points coincide to form the (n, m) nanotube. Thus armchair, zig-zag and chiral nanotubes can be represented as (n, n), (n, 0) and (n, m) respectively. Like many solids, carbon nanotubes are not devoid of defects. Such defects in carbon nanotubes at the intramolecular junction, formed by interposing one or more topological pentagon/heptagon defects in the hexagonal structure between two nanotube segments of different helicity was predicted first theoretically [29] and observed later experimentally [30]. Depending on the orientation in the hexagonal network, the pentagon-heptagon pairs can create a small deformation in the nanotube. It is considered to be a local defect in a straight nanotube. Defects in nanotubes can be produced by controlled electron irradiation, for example. This causes atom removal and creates vacancies, which cluster into large holes in the structure. Molecular simulations have shown that such nanotubes undergo surface reconstruction and nonhexagonal rings such as squares, pentagons, heptagons and octagons so formed disappear finally through Stone-Wales mechanism and lead to five-, six-, and seven membered rings [31]. Coalescence and welding of carbon nanotubes have also been reported [32]. Welding of nanotubes creates molecular junctions of various geometries like X, Y and T [33, 34]. These defects in carbon nanotubes seem to be responsible for the changes in many of their properties. The mechanical properties of carbon nanotubes have been discussed extensively in the last 1 decade. The Young's modulus and tensile strengths of carbon nanotubes are very high compared to that of steel. Reinforcement of these carbon nanotubes can be done to fully exploit the above tensile strengths by the coiling of the tubes. Many models have been proposed for these coiled nanotubes. Recently, Szabó et al. [35] reported the inclusion of impurities like N and S atom and non-hexagonal rings causing the coiling of carbon nanotubes. The folding of haeckelite sheets, which are made up of pentagon, hexagon and heptagons, has also been predicted. All the proposed models explain either the local defect in the straight nanotube or the non-uniform coils of carbon nanotube.

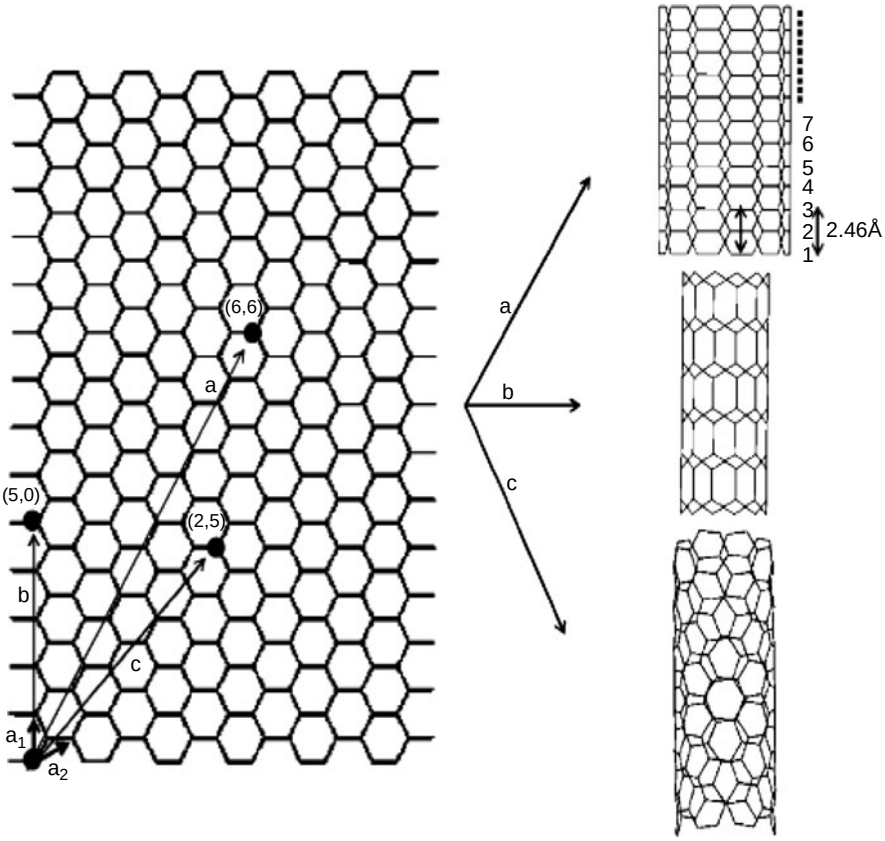

Fig. 12 Rolling of a graphite layer to form single-walled carbon nanotubes of (**a**) armchair, (**b**) zig-zag and (**c**) chiral type. The numbering in the case of the armchair nanotube shows the numbering of the layers running perpendicular to the tube axis as described in the text

3.10 Catalyst Nanoparticles for Carbon Nanotubes

Catalysts speed up chemical reactions but can be recovered unchanged at the end of the reaction. They can also direct the reaction towards a specific product and allow chemistry to be carried out at lower temperature and pressures with higher selectivity towards the desired product. As a result they are used very extensively in chemical industry. There are two kinds of catalysts. Heterogeneous catalysts are insoluble in the medium in which the reaction is taking place so that reactions of gaseous or liquid reagents occur at the surface, whilst homogeneous catalysts are dissolved in the reaction medium and hence all catalytic sites are available for reaction. Some of the properties of catalysts are collected in Table 3, where homogenous and heterogeneous catalysts are compared.

Table 3 Comparison of homogeneous and heterogeneous catalysts [36]

	Heterogeneous	Homogeneous
Catalyst from	Solid, often metal or metal oxide	Metal complexes
Mode of use medium	Fixed bed or slurry	Dissolved in reaction
Solvent	Usually not required	Usually required – can be product or byproduct
Selectivity	Usually poor	Can be tuned
Stability	Stable to high temperature	Often decompose $<100°C$
Recyclability	Easy	Can be very difficult
Special reactions	Haber process, exhaust clean up etc	Hydroformylation of alkenes, methanol carbonylation, asymmetric synthesis etc

The *d*-orbital transition metals known to have strong catalyst activity in general [37]. Transition metal carbides and nitrides are used in a wide range of applications due to their unique physical and chemical properties [38]. They also exhibit high catalytic activity in different reactions including hydrogenation [39–41], hydrodesulfurization and hydrodenitrogenation [42–46].

The catalytic properties of metals should be regarded as only one of the physical and chemical properties of metals requiring theoretical interpretation. The difficulties encountered in developing a satisfactory theory of the metallic state are well known. Two extreme types of theory have been proposed: in the Electron Band, electrons are assumed to be delocalized over the whole metallic crystal, but at least in its simplest form. This theory cannot account for the regular variation in crystal structure across the Transition Series. While for the Valence Bond Theory, in which the cohesive properties of metals are described in terms of localized bonds between atoms, has been extended to describe this phenomenon [47]. Both theories have been of some assistance in accounting for catalytic properties, but both have their limitations. It is therefore worth examining whether the description of metallic behavior in terms of molecular orbitals is fruitful when applied to surface phenomena. It is worth emphasizing that these new approach, due especially to Good-enough [48], is not a completely new theory [49] but rather an attempt to unify the two theories mentioned above. It applies to the molecular orbital theory: it is best described in relation to the face-centered cubic metals to which family belong most of the metals of catalytic interest. In these metals each atom is in contact with 12 others, four in each of three planes mutually at right angles, while six others octahedrally disposed lie at a slightly greater distance. According to the Crystal Field Theory the five d-orbitals are split in an octahedral environment into two groups.

The two higher energy orbitals are taken to lie along the Cartesian axes (Fig. 13a) and are designated $d_{x^2-y^2}$ and d_{z^2}, or collectively in the language of group theory as e_g. The three lower energy orbitals then lie between the Cartesian axes (Fig. 13b) and so are designated d_{xy}, d_{yz} and d_{xz} or collectively as t_{2g}. As each of these orbitals has four lobes, it is reasonable to say that the 12 near neighbours in the face-centered

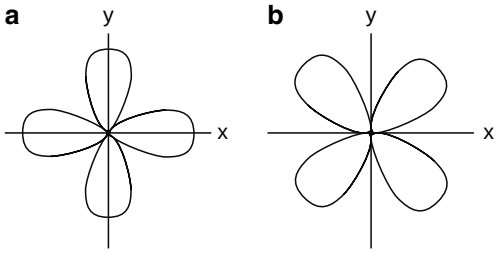

Fig. 13 Representation of (**a**) the $d_{x^2-y^2}$ orbital and of (**b**) the d_{xy} orbital, examples respectively of the e_g and t_{2g} families of orbitals in an octahedral complex

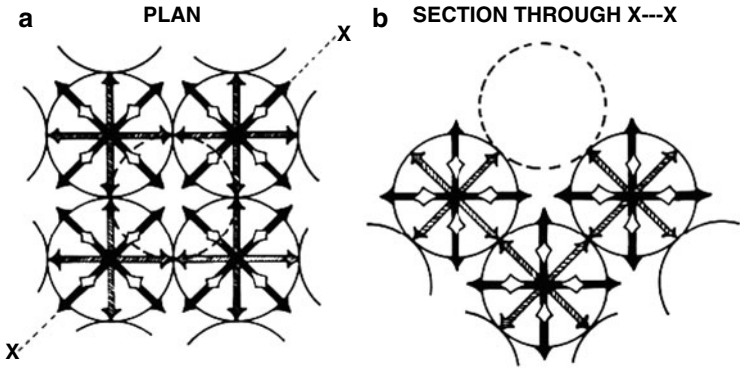

Fig. 14 The emergence of orbitals from the (100) face of a face-centered cubic metal: (**a**) plan; (**b**) section; *Filled arrows*: e_g orbitals in plane of paper, *Hatched arrows*: t_{2g} orbitals in plane of paper, *Open arrows*: t_{2g} orbitals at 45° to plane of paper

cubic crystal are bonded to the central atom by t_{2g} orbitals which overlap to form a broad collective t_{2g} band, while the *six* next nearest neighbours are bonded by e_g orbitals. In fact, however, these latter orbitals do not overlap significantly because the next nearest neighbours are too far apart, so that electrons in the e_g orbitals occupy localized states around each atom. It is now an easy matter to evaluate the manner in which the two groups of orbitals emerge from the three low index planes. This is illustrated in Figs. 14 and 15 for the (100) and (110) planes respectively.

The former consists of a square array of atoms (Fig. 14a): the non-bonding e_g orbitals in the plane of the surface are shown in black while the bonding t_{2g} orbitals are hatched. Furthermore, there are four t_{2g} orbitals emerging from each atom at 45° to the plane of the surface, and these are shown in white: one of these from each of four atoms is directed towards the position occupied by an atom in the next layer. Figure 14b shows a section normal to the surface. Figure 15a shows the plan of the (110) plane: this consists of parallel rows of next nearest neighbors bonded as usual by shaded t_{2g} orbitals. Other t_{2g} orbitals emerge, four from each atom (shown in white) at 30° to the plane of the surface and are directed towards the sites of atoms in the next layer. Figure 15b shows a section normal to the surface: this plane differs

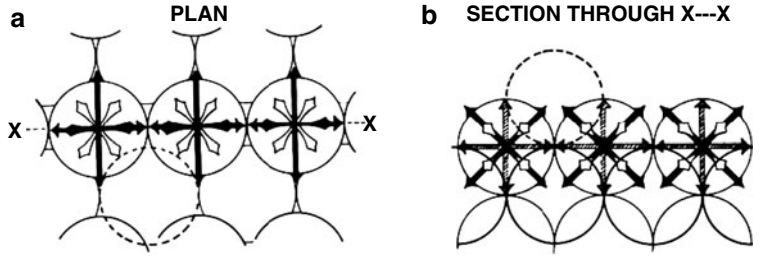

Fig. 15 The emergence of orbitals from the (110) face of a face-centered cubic metal: (**a**) plan; (**b**) section; *Filled arrows*: e_g orbitals in plane of paper or emerging at 45°, *Hatched arrows*: t_{2g} orbitals in plane of paper, *Open arrows*: t_{2g} orbitals at 30° to plane of paper

from the (100) in that it is a t_{2g} orbital which emerges normal to the surface from each atom. Having obtained the direction of emergence of the t_{2g} and e_g orbitals from the low index planes of the crystal, it is now necessary to try to decide on the extent: to which they are occupied by electrons. If in Group VIII, (nickel, palladium and platinum), according to Goodenough [48], the 0.55 d-band holes are distributed between the two bands as follows : t_{2g} band, 0.41 holes: e_g band, 0.14 holes. Both bands are therefore substantially filled, and supposed that both can participate in forming covalent bonds with adsorbed species. The atom in the centre foreground is deeply imbedded in the surface: it is bonded by overlap of its spherical 1s orbital with four e_g orbitals from the surrounding metal atoms and by a further e_g orbital from the metal atom below it. This must therefore be quite a strongly bound state. The atom on the left is bonded only by this latter e_g orbital and is likely to be much more weakly bound. The atoms on the left and right are bonded simply by the normal-emergent t_{2g} orbitals: the one on the right is, however, bonded to a metal atom in a layer one below the surface, but both should be weak states of binding. The position of the atom in the centre is more complicated: it is bonded by two t_{2g} orbitals emerging from the atoms below it and by two e_g orbitals emerging from the atoms below it and by two e_g orbitals from the atoms on either side of it. This should therefore be a strongly bound state. Space does not permit the elaboration of these ideas to the adsorption of other atoms and molecules.

Mostly 3d-metals are used to catalyze formation of CNTs because of their ability to decompose hydrocarbons. However, they are not all equivalent and, in particular, alloying them with each other or with other non-transition metals dramatically changes (generally improves) their catalytic properties. The role of the non-transition metal is to disperse and to stabilize the catalyst metal-so an effect on the geometric aspect (for example, support catalyst). On the other hand, effects of alloying two/three transition metals on e.g. the electronic structure or the carbon solubility and diffusion, observed improvement in the catalyst performances as studied here. Furthermore, overlap of catalyst 3d-orbitals with carbon orbitals after hydrocarbon dissociation could be a relevant parameter for the CNT growth process. The link between the size of the catalyst nanoparticles and the diameter

of the CNTs and the consequently absolute necessity to prepare stable nanoparticles of controlled size has been emphasized. To meet this severe constraint high-technological efforts have to be made. Though, other parameters concerning the catalyst morphology have an influence on the growth process like the crystallographic orientation of the nanoparticles. The preparation method of the catalyst particles also plays its part in the complex problem of the factors influencing the catalytic properties of the metal nanoparticles. The choice of the preparation method determines the morphology of the obtained nanoparticles and the use of porous support to limit the size of the nanoparticles. But the influence of the preparation method is not limited to morphological effects and can directly affect catalytic properties. A given catalyst can yield completely different results upon CVD when supported on different materials. So not only the catalyst has to consider but the catalyst/support. The interactions between catalyst and support are found to be essential. First, they partly determine the morphology of the nanoparticles and, second, they also alter the electronic structure of the nanoparticles, which altering their catalytic properties. These interactions depend on both support and catalyst materials but also on their crystallographic orientations, on the surface roughness and porosity of the support. Finally, pretreatment can be essential for activating the catalyst by reducing it to its actual catalytic form (pure metal) or by forming nanoparticles from the annealing. Moreover, the parameters concerning the catalyst nanoparticles only cannot explain whether CNTs will grow or not and how they will grow. The catalytic process requires a hydrocarbon gas (or CO) coupled with a supported catalyst in charge of its dissociation and the subsequent growth of the CNT. The catalyst/gas or rather the trio support/catalyst/gas should be considered for a complete understanding of the growth process. Other important factors influence the kinetic and thermodynamic aspects of the growth process, e.g. temperature, pressure, flow rate and reaction time. Many authors explain their success in producing SWNTs by the very small size of their catalyst nanoparticles. However, the differentiation between SWNT and MWNT growth processes is not really clear and kinetic arguments are often invoked.

3.11 Preparation of Carbon Nanotubes

Here, we presented result of carbon nanotubes synthesized by a newly developed method; fluidized floating catalyst method [23] as shown in Fig. 16.

The growth of CNTs was carried out in a tubular furnace with a horizontal quartz tube at atmospheric pressure using fluidized floating catalyst method. Firstly, carrier gas (Argon) was flushed for about 10 min before the furnace was turned on to remove the surrounding air and to create an inert atmosphere. Then, the precursor (camphor oil) and catalyst (Fe/Co/Al) mixtures with ratio (1:1:1) were placed together in a quartz boat and pushed into the center of the quartz tube. Then the quartz tube was heated in Ar ambient with a flow rate of 50 sccm to ensure no oxygen. When the temperature of the furnace rapidly increased to 650°C, it was

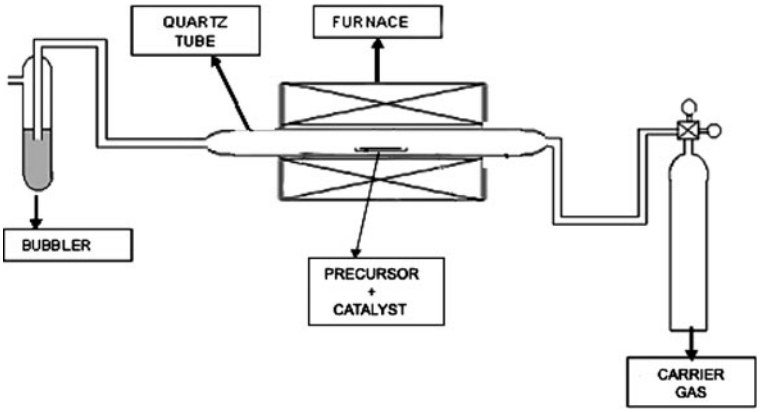

Fig. 16 A schematic sketch of modified fluidized floating catalyst method [23]

discovered that CNTs were deposited in the quartz boat. Carbon deposited materials formed were removed from the catalyst boat. The temperature was maintained for a further period of 30 min for annealing process after deposition. Finally, the quartz tube was cooled down to room temperature in Ar ambient with a flow rate of 50 sccm. The carbon deposited materials formed were removed from the quartz boat.

3.11.1 Surface Morphology

The FESEM micrograph shows the CNTs grown was randomly curled as shown in Fig. 17. When camphor oil decomposed into vapor state, CNTs was found to be deposited in the presence of catalyst. From here, we noticed the conversion of carbon to CNT was dependent on the amount of catalyst used. Different percentage of catalyst used to deposit CNTs which are 0.25% (FCM1), 0.50% (FCM2), 0.75% (FCM3), 1.00% (FCM4) and 1.25% (FCM5) [23]. The CNTs yield was estimated by weighing the amount of CNTs obtained and it was found to be the highest at 0.75% of catalyst. Therefore, 0.75% Fe/Co/Al can be considered as optimum catalyst concentration for CNTs synthesized by fluidized floating catalyst method.

The morphology of CNTs investigated by Samant et al. [50] on effects of ferrocene using naphthalene as precursor by Thermal-CVD method observed spider-like web structure CNTs. The SEM recorded on the product formed in the presence of Ar gas is shown in Fig. 18.

As seen, the substrate is occupied with densely packed, CNTs with average tube-diameter of about 70 nm. Not much variation in size or packing density was observed in the micrographs recorded at various other areas. Small amount of amorphous carbon in the form of globules (as marked with red arrow) is also seen in the picture. The bright, spherical structures at one of the ends of most of the tubes are attributed to the iron nanoparticles formed by decomposition of

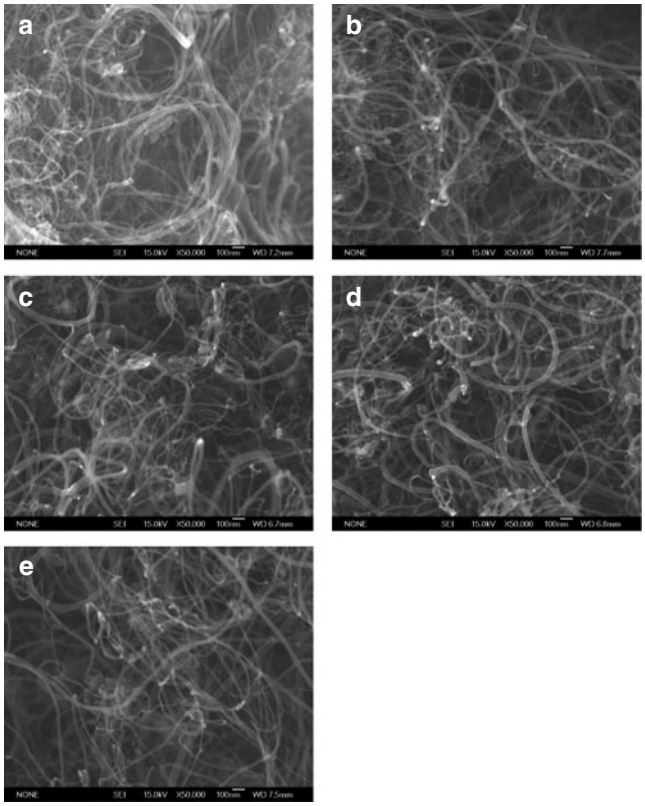

Fig. 17 FESEM images of CNTs using (**a**) 0.25% (FCM1), (**b**) 0.50% (FCM2), (**c**) 0.75% (FCM3), (**d**) 1.00% (FCM4) and (**e**) 1.25% (FCM5) of catalyst (Fe/Co/Al) by fluidized floating catalyst method [23]

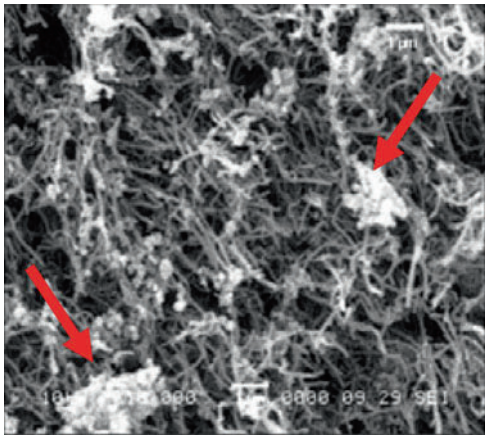

Fig. 18 SEM image of the CNTs deposited on fused silica plate in the presence of Ar [50]

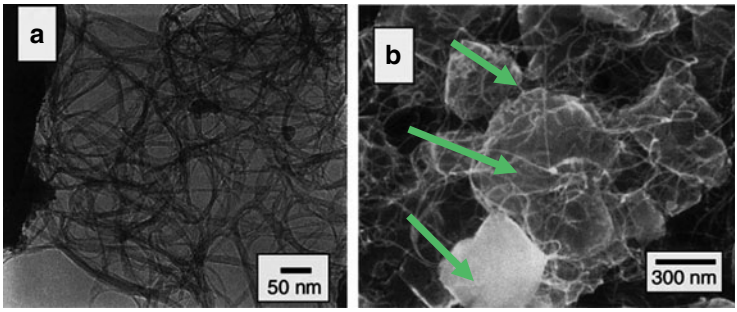

Fig. 19 Lower magnification TEM image (**a**) and SEM image (**b**) of 'as grown' SWNTs [51]

ferrocene [50]. By using alcohol as the carbon source, a new simple catalytic chemical vapor deposition technique to synthesize high purity single-walled carbon nanotubes at low temperature is demonstrated by Maruyama et al., [51] at 550°C. The morphology of the deposited CNTs is shown in Fig. 19.

In brief, iron and cobalt acetate were dissolved in ethanol and mixed with Y-type zeolite powder. The amounts of Fe and Co were 2.5 wt% each. From the SEM image in 19(b), a small amount of 'as grown' sample was placed with a conductive tape used for the observation. Here, web-like growth of bundles of SWNTs also observed from zeolite particles around 300 nm. However, no other structures such as amorphous carbon are observed from both (a) and (b) except the zeolite flakes (as marked with green arrow) which used as the support catalyst. The impurities such as amorphous carbon, multi-walled carbon nanotubes, metal particles and carbon nanoparticles are completely suppressed even at relatively low reaction temperature due to the etching effect of decomposed OH radical attacking carbon atoms with a dangling bond. The high-purity synthesis at low temperature promises large scale production at low cost and the direct growth of SWNTs on conventional semiconductor devices already patterned with aluminum [51].

The role of catalyst can yield completely different results upon CVD when supported on different materials. So not only the catalyst has to consider but the catalyst/support. The interactions between catalyst and support are found to be essential. First, they partly determine the morphology of the nanoparticles and, second, they also alter the electronic structure of the nanoparticles, which altering their catalytic properties. These interactions depend on both support and catalyst materials but also on their crystallographic orientations, on the surface roughness and porosity of the support. Finally, pretreatment can be essential for activating the catalyst by reducing it to its actual catalytic form (pure metal) or by forming nanoparticles from the annealing. Moreover, the parameters concerning the catalyst nanoparticles only cannot explain whether CNTs will grow or not and how they will grow. The catalytic process requires a hydrocarbon gas (precursor) with a supported catalyst in charge of its dissociation and the subsequent growth of the CNT. The catalyst/gas or rather the trio support/catalyst/gas should be considered for a

complete understanding of the growth process. Other important factors influence the kinetic and thermodynamic aspects of the growth process, e.g. temperature, pressure, flow rate and reaction time. However, the differentiation between SWNT and MWNT growth processes is not really clear and kinetic arguments are often invoked.

Tao et al. [52] also employed ferrocene as catalyst but interestingly as precursor as well. CNTs have been synthesized via directly pyrolyzing only as the precursor in the autoclave. The nanotubes with several micrometers in length have outer and inner diameters in the range of 40–100 nm and 2–40 nm, respectively. Yield of ~70% of CNTs can be obtained without any accessorial solvents and catalysts. Experimental results showed that a temperature higher than 600°C in conjunction with proper pressure was favorable for achievement of the nanotubes [52]. Figure 20a, b show SEM and TEM images of carbon nanotubes, respectively. It can be seen that large quantity of nanotubes can be achieved by this method.

The yield of carbon nanotubes estimated through SEM and TEM observations of the as-prepared samples was 70%. Most of the carbon nanotubes with close ends and curly morphologies have outer diameters of 40–100 nm, inner diameters of 20–40 nm and length up to several micrometers, and no metal catalyst particles were detected from TEM image (Fig. 20b). The size of the catalyst nanoparticles seems to be the determining factor for the diameter of the CNT grown on it. Beyond this size correlation, only small nanoparticles are able to catalyze formation of CNT. This can be explained on the one hand by the fact that such very small nanoparticles can exhibit peculiar electronic properties and thus catalytic properties due to the unusual high ratio surface atom/bulk atom. On the other hand, the growth mechanism involving the formation of a carbon cap on the nanoparticle surface to reduce its unusual high surface energy. The crystallographic orientation of the catalyst nanoparticle too can be crucial for CNT growth.

Pawan et al., deposited CNTs by chemical vapor deposition [53]. Methane (CH_4) and hydrogen (H_2) were used as precursor gases for the CNT growth with Ni as the catalyst. Figure 21 shows the SEM micrograph of the as-grown CNTs deposited

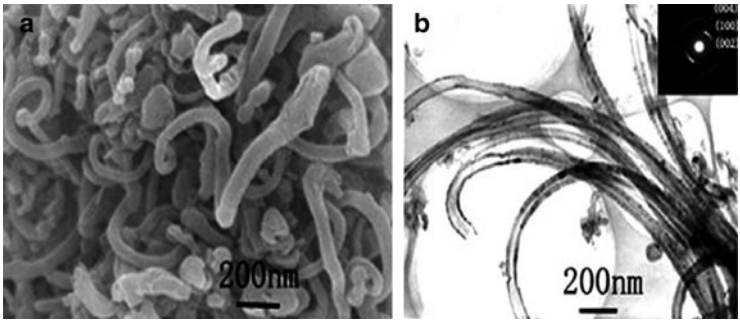

Fig. 20 (**a**) SEM image and (**b**) TEM image of the carbon nanotubes; (inset 3b) SAED pattern of individual carbon nanotube [52]

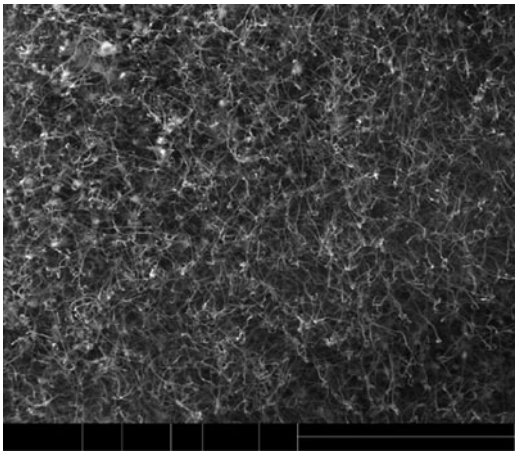

Fig. 21 SEM micrograph of the as-grown CNTs deposited using the CVD method [53]

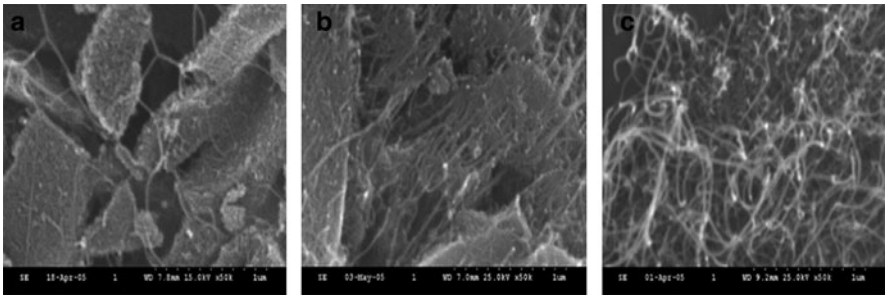

Fig. 22 SEM images of CNTs grown on catalysts with different Mo concentrations: (**a**) Fe:Mg:Mo = 0.1:12:0.1, (**b**) Fe:Mg:Mo = 0.1:12:0.5, and (**c**) Fe:Mg:Mo = 0.1:12:1 [54]

using CVD. The tubes were long, dense and showed a typical MWNTs structure. By using Ni as the catalyst, the area density of the deposited CNTs was high and the tubes appeared parallel to the substrate.

Mixing of two or more different metal catalysts yields improvement of the catalyst performance in terms of quality of obtained product or lowering the reaction temperature. Study on the effect of Fe catalyst with different ratio of Mo and Mg was investigated by Yangfang et al. [54]. High quality, high yield CNTs were synthesized on a composite catalyst using catalytic chemical vapor deposition. The composite catalysts Fe/MgO, Mo/MgO and (Fe, Mo)/ MgO, prepared via the sol gel method using citric acid as fuel, were investigated for the production of CNTs. Only the (Fe, Mo)/MgO catalyst could support CNTs growth with high yield in this study. The different mole ratios between Fe, Mo, and Mg resulted in changes in product structure, diameter size, and yield. Decreasing the Fe concentration reduces the structural defects, and by increasing the Mo concentration, the yields of CNTs clearly increase as observed in Fig. 22.

The influence of catalyst composition on the growth of CNTs was studied in this paper. Among the four catalysts, Fe-Mg-O, Fe-Mo-O, Mg-Mo-O, and Fe-Mg-Mo-O, made by the sol-gel method, only Fe-Mg-Mo-O supported the production of CNTs with high yield. In the catalyst, Fe was considered as the catalytic center to magnetize carbon atoms for the CNTs growth, but the crystallite size of Fe was very important in carbon nanofibers growth. The larger the Fe particle size, the more carbon nanofibers were formed as the size of the catalyst nanoparticle is important to determine the diameter of the nanotubes. By controlling the Fe concentration in the catalyst was necessary in preparing CNTs with few carbon nanofibers and in simultaneously controlling the diameter of the CNTs. Mo in the catalyst Fe-Mg-Mo-O was proved to accelerate carbon depositing, which favored the high yield of CNTs. Higher Mo concentration facilitated the structural transformation from carbon soot to carbon nanotubes. The ratio harmony of the metal element and crystallite size of the particles in the composite catalyst were very important. The catalyst composition Fe:Mg:Mo = 0.1:12:1 in our study was successful in CNTs growth with high yield, high purity, fewer walls, and smaller diameter [54].

3.12 Applications of Carbon Nanotubes

CNTs have extraordinary electrical conductivity, heat conductivity and mechanical properties. They are probably the best electron field-emitter possible. They are polymers of pure carbon and can be reacted and manipulated using the tremendously rich chemistry of carbon. This provides opportunity to modify the structure and to optimise solubility and dispersion. Very significantly, CNTs are molecularly perfect, which means that they are free of property-degrading flaws in the nanotube structure. Their material properties can therefore approach closely the very high levels intrinsic to them. These extraordinary characteristics give CNTs potential in numerous applications.Here, we discussed the application of CNTs in electrochemical system.

3.12.1 Lithium-Ion Battery

The outstanding mechanical properties and the high surface-to-volume ratio (due to their small diameter) make carbon nanotubes potentially useful as anode materials [55–60] or as additives [61] in lithium-ion battery systems. An electrode containing 10 wt% of carbon nanotubes as the additive displays a homogeneous distribution of nanotubes in synthetic graphite. The cyclic efficiency of a synthetic graphite anode as a function of the weight percent of carbon nanotube. With increasing weight percent of carbon nanotubes, the cyclic efficiency of the synthetic graphite battery anode increases continuously, and, in particular, when 10 wt% of the nanotubes was added, the cyclic efficiency was maintained at almost 100% up to 50 cycles. At

higher concentrations, the nanotubes interconnect graphite powder particles together to form a continuous conductive network.

3.12.2 Additives to the Electrodes of Lead-Acid Batteries

In order to increase the conductivity of electrodes in lead-acid batteries, different weight percents of carbon nanotubes are added to the active anode material (with average diameters of ca. 2–5 mm) of the positive electrode. The resistivity of the electrode is lowered for the case of 1.5% nanotube addition. When this sample (0.5–1 wt%) is incorporated in the negative electrode, the cycle characteristics are greatly improved compared with those of an electrode without additive [61]. This is probably due to the ability of carbon nanotubes to act as a physical binder, resulting in electrodes that undergo less mechanical disintegration and shedding of their active material. Therefore, it is expected that the use of carbon nanotubes as an electrode's filler should produce an enhanced cyclic behavior for electrodes in lead-acid batteries compared with electrodes using conventional graphite powder, because the unusual morphology of the carbon nanotube, such as the concentric orientation of their graphite crystallites along the fibre cross-section, induces a high resistance towards oxidation, and furthermore the nanotube network embedded in the polymer would enhance the reactivity of the electrode.

3.12.3 The Electric Double-Layer Capacitor

The merit of the electric double-layer capacitor (EDLC) is considered to be a high discharge rate [62], which makes them applicable as a hybrid energy source for electric vehicles and portable electric devices [63]. EDLCs containing carbon nanotubes in the electrode exhibit relatively high capacitances resulting from the high surface area accessible to the electrolyte [60, 64, 65]. On the other hand, the most important factor in commercial EDLCs is considered to be the overall resistance. In this context, carbon nanotubes with strong electrical and mechanical properties can be used as an electrical conductive additive in the electrode of EDLC. It has been demonstrated that the addition of carbon nanotubes results in an enhanced capacity at higher current densities, when compared with electrodes containing carbon black [66].

3.12.4 Fuel Cells

Fuel cells have been considered as the next generation of energy devices because this type of system transforms the chemical reaction energy from hydrogen and oxygen into electric energy [67]. Carbon nanotubes decorated with metal nanoparticles as the electrode have doubled the performance of the fuel cell, owing to the increased catalytic activity of nanotube-based electrodes [68–70]. In this context,

we have reported the efficient impregnation of Pt nanoparticles (outer diameter less than 3 nm) on cup-stacked type carbon nanotubes [71]. The method involves dispersion of the fibers in H_2PtC_{16}, followed by low-temperature annealing. The Pt particle deposition is always homogeneous, and can be controlled selectively on the outer or inner core using the hydrophobic nature of the material. Since the Pt particle activity on the fibers is high, this material could find application as an efficient catalyst or biological device. It may be that carbon nanotube technology will contribute to the development of fuel cells as a catalyst support and also as a main component of bipolar systems. However, additional basic and applied research is necessary.

3.12.5 Multifunctional Fillers in Polymer Composite

It has been shown that carbon nanotubes could behave as the ultimate one-dimensional material with remarkable mechanical properties [72, 73]. The density-based modulus and strength of highly crystalline SWNTs are 19 and −56 times that of steel. Based on a continuum shell model, the armchair tube exhibits larger stress-strain response than the zigzag tube under tensile loading. Strong mechanical properties of carbon nanotubes due to a strong carbon-carbon covalent bond are highly dependent upon the atomic structure of nanotubes and the number of shells. Moreover, carbon nanotubes exhibit strong electrical and thermal conducting properties. Therefore, carbon nanotubes (single and multi-walled) have been studied intensively as fillers in various matrices, especially polymers [74–78]. The best use of the intrinsic properties of these fibrous nanocarbons in polymers can be achieved by optimizing the interface interaction of the nanotube surface and the polymer. Therefore, surface treatments via oxidation could be used in order to improve adhesion properties between the filler and the matrix. This results in a good stress transfer from the polymer to the nanotube. There are various surface oxidative processes, such as electrochemical, chemical and plasma techniques. From the industrial point of view, ozone treatment is a very attractive technique. In addition, the dispersion of the nanotubes/nanofibres in the polymer should be uniform within the matrix.

The smallest working composite gear has been prepared by mixing nanotubes into molten nylon and then injecting into the tiny mould. As shown in Fig. 12, this gear is as small as the diameter of a human hair. This piece exhibits a high mechanical strength, high abrasion resistance and also good electrical and thermal conductivity. When cup-stacked-type carbon nanotubes are incorporated in polypropylene, the improvement of the tensile strength is very noticeable (up to 40%). This remarkable result can be explained by the particular morphology of cup-stacked-type carbon nanotubes. In other words, a large portion of edge sites on the outer surface of the nanotubes might act as nucleation sites, resulting in good adhesion between nanotubes and polymers (good stress transfer). Recently, various studies on the nucleation effect of nanotubes on the crystallization of semi-crystalline polymers have been reported [79–81].

4 Conclusion

Carbon materials have various forms, crystalline and non-crystalline carbon constitutes a class of new materials with a wide range of compositions, properties, and performance. Carbon based material can be prepared by a variety of techniques such as CVD, PLD etc. Due to its unique optical and electrical properties, carbon has potential applications in various fields especially in semiconductor devices. Many interesting crystalline phases with useful properties have been predicted which make carbon promising target for preparative materials scientists and chemists. The majority of the experimental approaches are based on vapor phase deposition routes, which furnished many interesting properties. This chapter has shown the effect of the catalyst on the morphology of the carbon nanotubes. The size, substrate and the composition of the catalyst seems to be the determining factors on the formation and diameter of the nanotubes. Interactions between catalyst and support are essential since they can greatly affect the electronic structure of the nanoparticles and their morphology and in turn their catalytic properties. Hence, selecting the best catalyst and substrate is crucial to synthesize carbon nanotubes. In summary it can be stated that a fascinating new field in the area of carbon has been discovered, which gives motivation for further studies dedicated to fundamental questions as well as the exploitation of the novel materials for future industrial applications.

Acknowledgment The author would like to thank NANO-SciTech Centre and Faculty of Applied Sciences, UiTM and RMI, UiTM for the facilities and financial support on this project.

References

1. Allamandola, L.J., Hudgins, D.M., Bauschlicher Jr., C.W., Langhoff, S.R.: Astron. Astrophys. **352**, 659–664 (1999)
2. Kroto, H.W., Heath, J.R., O'brien, S.C., Curl, R.F., Smalley, R.E.: Nature **318**, 162–163 (1982)
3. Iijima, S.: Nature **354**(6348), 56–58 (1991)
4. Yakobson, B.I., Smalley, R.E.: Am. Sci. **85**, 324–337 (1997)
5. Kroto, H.W., Allaf, A.W., Balm, S.P.: Chem. Rev. **91**, 1213–1235 (1991)
6. Kraetschmer, W., Lamb, L.D., Fostiropoulos, K., Huffman, D.R.: Nature **347**, 354–58 (1990)
7. Haufler, R.E., Coceicao, J., Chibante, L.P.F., Chai, Y., Byrne, N.E., et al.: J. Phys. Chem. **94**, 8634–8640 (1990)
8. Dresselhaus, M.S., Dresselhaus, G., Eklund, P.C.: Science of Fullerenes and Carbon Nanotubes. Academic, San Diego (1996)
9. Dresselhaus, M.S., Gresselhaus, G., Sugihara, K., Spain, I.L., Goldberg, H.A.: Graphite Fibers and Filaments, vol. 5. Springer Series in Materials Science, Springerverlag, Berlin (1988)
10. Lahaye, J., Prado, G.: In: Walker Jr, P.L. (ed.) Chemistry and Physics of Carbon, vol. 16. Marcel Dekker, New York (1978)
11. Donnet, J.B., Bansal, R.C., Wang, M.J.: Carbon Black. Marcel Dekker, New York (1993)
12. McClure, J.W.: In: Carter, D.L., Bate, R.T. (eds.) Proceeding of the International Cong. On Semimetals and Narrow Gap Semiconductors. Pergamon, New York (1971)

13. Charlier, J.J.C.: PhD thesis, Dept. of Phys. Mater., Catholic Univ. of Louvain (1994)
14. Hauser, J.J.: Solid State Commun. **17**, 1577–1580 (1975)
15. Bubenzer, A., Dischler, B., Brandt, G., Koidi, P.: J. Appl. Phys. **54**, 4590–4595 (1983)
16. Ebbesen, T.W.: Carbon Nanotubes. CRC, Boca Raton, New York, London, Tokyo (1997)
17. Ruffieux, P.: Thesis, University of Fribourg, Switzerland (2002)
18. Rohlfing, E.A., Cox, D.M., Kaldor, A.: J. Chem. Phys. **81**, 3322–3330 (1984)
19. Carman, H.S., Compton, R.N.: J. Chem. Phys. **98**, 2473–2476 (1993)
20. Kroto, H.W., Heath, J.R., O'Brien, S.C., Curl, R.F., Smalley, R.E.: Nature **318**, 162–163 (1985)
21. Dresselhaus, M.S., Dresselhaus, G., Saito, R.: Carbon **33**, 883–891 (1995)
22. McEnaney, B.: In: Burchell, T.D. (ed.) Carbon Materials for Advanced Technologies. Pergamon, Amsterdam, Lausanne, New York, Oxford, Shannon, Singapore, Tokyo (1999)
23. Azira, A.A., Zainal, N.F.A., Nik, S.F., Mohamad, F., Kudin, T.I.T., Soga, T., Abdullah, S., Rusop, M.: Mater. Res. Innovat. **13**(3), 182–184 (2009)
24. Azira, A.A., Zainal, N.F.A., Nik, S.F., Rusop, M.: AIP Conf. Proc. **1136**, 720–724 (2009)
25. Azira, A.A., Zainal, N.F.A., Nik, S.F., Rusop, M.: AIP Conf. Proc. **1136**, 735–739 (2009)
26. Azira, A.A., Zainal, N.F.A., Nik, S.F., Rusop, M.: AIP Conf. Proc. **1136**, 740–744 (2009)
27. Azira, A.A., Zainal, N.F.A., Nik, S.F., Soga, T., Abdullah, S., Rusop, M.: Int. J. Nanosci. **8**(4 & 5), 351–357 (2009)
28. Hamada, N., Sawada, S., Oshiyama, A.: Phys. Rev. Lett. **68**, 1579–1581 (1992)
29. Dunlap, B.I.: Phys. Rev. B **46**, 1933–1936 (1992)
30. Amelinckx, S., Zhang, X.B., Bernaerts, D., Zhang, X.F., Ivanov, V., Nagy, J.B.: Science **265**, 635–639 (1994)
31. Ajayan, P.M., Ravikumar, V., Charlier, J.C.: Phys. Rev. Lett. **81**, 1437–1440 (1998)
32. Charlier, J.C.: Acc. Chem. Res. **35**, 1063–1069 (2002)
33. Terrones, M., Banhart, F., Grobert, N., Charlier, J.C., Terrones, H., Ajayan, P.M.: Phys. Rev. Lett. **89**(075505), 1–4 (2002)
34. Deepak, F.L., Govindaraj, A., Rao, C.N.R.: J. Chem. Sci. **118**, 9–14 (2006)
35. Szabó, A., Fonseca, A., Nagy, J.B., Lambin, Ph, Biro, L.P.: Carbon **43**, 1628–1633 (2005)
36. Saito, R., Takeya, T., Kimura, T.: Phys. Rev. **B 57**, 4145–4153 (1998)
37. Cole Hamilton, D.J., Tooze, R.P.: Catalysis by Metal Complexes, vol. 30. Springer, Netherlands (2006)
38. Atkins, P.W.: Physical Chemistry, 6th edn. W.H. Freeman & Co., New York (1997)
39. Oyama, S.T.: The Chemistry of Transition Metal Carbides and Nitrides. Blackie Academic and Professional, London (1996)
40. Lee, J.S., Yeom, M.H., Park, K.Y., Nam, I.S., Chung, J.S., et al.: J. Catal. **128**, 126–136 (1991)
41. Oyama, S.T.: Catal. Today **15**, 179–200 (1992)
42. DaCosta, P., Lemberton, J.L., Potvin, C., Manoli, J.M., Perot, G., et al.: Catal. Today **65**, 195–200 (2001)
43. Liaw, S.J., Raje, A., Chary, K.V.R., Davis, B.H.: Appl. Catal. A Gen. **123**, 251–271 (1995)
44. Raje, A., Liaw, S.J., Chary, K.V.R., Davis, B.H.: Appl. Catal. A Gen. **123**, 229–250 (1995)
45. Ramanathan, S., Oyama, S.T.: J. Phys. Chem. **99**, 16365–16372 (1995)
46. Sajkowski, D. J., Oyama, S. T.: ACS Div. Fuel Chem. Preprints **35**(2), 233–236 (1990)
47. Melo-Banda, J.A., Dominguez, J.M., Sandoval-Robles, G.: Catal. Today **65**, 279–284 (2001)
48. Altmann, S.L., Coulson, C.A., Hume-Rothery, W.: Proc. R. Soc. A **240**, 145–159 (1957)
49. Goodenough, J.B.: Magnetism and the Chemical Bond. Interscience, New York (1963)
50. Samant, K.M., Haram, S.K., Kapoor, S.: J. Phys. **68**(1), 51–60 (2007)
51. Maruyama, S., Kojima, R., Miyauchi, Y., Chiashi, S., Kohno, M.: Chem. Phys. Lett. **360**, 229–234 (2002)
52. Tao, C., Zhiyong, F., Guifu, Z., Qixiu, H., Biao, H., Xiao, Z.Y., Youjin, Z.: Bull. Mater. Sci. **29**(7), 701–704 (2006)
53. Pawan, K.T., Singha, M.K., Abha, M., Umesh, P., Misraa, D.S., et al.: Thin Solid Films **469–470**, 127–130 (2004)
54. Yanfang, C., Doh, H.R., Yun, S.L.: Met. Mater. Int. **14**(3), 385–390 (2008)

55. Endo, M., Nakamura, J., Sasabe, Y., Takahashi, T., Inagaki, M.: Trans. IEE Jpn. **A115**, 349–356 (1995)
56. Tatsumi, K., Zaghib, K., Abe, H., Higuchi, S., Ohsaki, T., Sawada, Y.: J. Power Sources **54**, 425–427 (1999)
57. Frackowiak, E., Gautier, S., Gaucher, H., Bonnamy, S., Beguin, F.: Carbon **37**, 61–69 (1999)
58. Wu, G.T., Wang, C.S., Zhang, X.B., Yang, H.S., Qi, Z.F., He, P.M., Li, W.Z.: J. Electrochem. Soc. **146**, 1696–1701 (1999)
59. Gao, B., Kelinhammes, A., Tang, X.P., Bower, C., Wu, Y., Zhou, O.: Chem. Phys. Lett. **307**, 153–157 (1999)
60. Frackowiak, E., Beguin, F.: Carbon **40**, 1775–1787 (2002)
61. Endo, M., Kim, Y.A., Hayashi, T., Nishimura, K., Matushita, T., Miyashita, K., Dresselhaus, M.S.: Carbon **39**, 1287–1297 (2001)
62. Conway, B.E.: Electrochemical Supercapacitors – Scientific Fundamentals and Technological Applications. Kluwer Academic, Dordrecht (1999)
63. Miyadera, K.: Toyota Tech. Rev. **52**, 22–27 (2002)
64. Niu, C., Sickel, E.K., Hoch, R., Moy, D., Tennent, H.: Appl. Phys. Lett. **70**, 1480–1482 (1997)
65. An, K.H., Kim, W.S., Park, Y.S., Moon, J.M., Lim, S.C., Lee, Y.S., Lee, Y.H.: Adv. Mater. **11**, 387–392 (2001)
66. Takeda, T., Takahashi, R., Kim, Y.J., Koshiba, K., Ishi, K., Kasahi, T., Endo, M.: TANSO **196**, 14–18 (2001)
67. Williams, M.C.: Fuel Cells **2**, 87–91 (2001)
68. Britto, P.J., Santhanam, K.S.V., Rubio, A., Alonso, A., Ajayan, P.M.: Adv. Mater. **11**, 154–157 (1999)
69. Che, G., Lakshmi, B.B., Fisher, E.R., Martin, C.R.: Nature **393**, 346–349 (1999)
70. Yoshitake, T., Shimakawa, Y., Kuroshima, S., Kimura, H., Ichihashi, T., et al.: Physica B **323**, 124–126 (2002)
71. Endo, M., Kim, Y.A., Ezaka, M., Osada, K., Yanagisawa, T., Hayashi, T., Terrones, M., Dresselhaus, M.S.: Nano Lett. **3**, 723–726 (2003)
72. Lu, J.P.: J. Phys. Chem. Solids **58**, 1649–1652 (1997)
73. Li, F., Cheng, B.S., Su, G., Dresselhaus, M.S.: Appl. Phys. Lett. **77**, 3161–3163 (2000)
74. Ajayan, P.M., Stephan, O., Colliex, C., Trauth, D.: Science **265**, 1212–1214 (1994)
75. Lau, K.T., Hui, D.: Composites **B33**, 263–277 (2002)
76. Calvert, P.: Nature **399**, 210–211 (1999)
77. Aamedov, M.A., Kotov, N.A., Prato, M., Guldi, D.M., Wicksted, J.P., Hirsch, A.: Nat. Mater. **1**, 190–194 (2002)
78. Zhan, G.D., Kuntz, J.D., Wan, J., Mukherjee, A.K.: Nat. Mater. **2**, 38–42 (2003)
79. Valentini, L., Biagiotti, J., Kenny, J.M., Santucci, S.: Appl. Polym. Sci. **87**, 708–713 (2003)
80. Bhattacharyya, A.R., Sreekumar, T.V., Liu, T., Kumar, S., Ericson, L.M., Hauge, R.H., Smalley, R.E.: Polymer **44**, 2373–2377 (2003)
81. Cadek, M., Coleman, J.N., Barron, V., Hedicke, K., Blau, W.J.: Appl. Phys. Lett. **81**, 5123–5125 (2003)